Nano-particle based scattering layers for optical efficiency enhancement of organic light-emitting diodes and organic solar cells

Hong-Wei Chang,[1,2] Jonghee Lee,[1] Simone Hofmann,[1] Yong Hyun Kim,[1] Lars Müller-Meskamp,[1] Björn Lüssem,[1] Chung-Chih Wu,[2,a)] Karl Leo,[1,b)] and Malte C. Gather[1,c)]

[1]*Institut für Angewandte Photophysik, Technische Universität Dresden, George-Bähr-Straße 1, 01062 Dresden, Germany*

[2]*Graduate Institute of Electronics Engineering, Graduate Institute of Photonics and Optoelectronics, and Department of Electrical Engineering, National Taiwan University Taipei 106, Taiwan*

(Received 25 February 2013; accepted 2 May 2013; published online 22 May 2013)

The performance of both organic light-emitting diodes (OLEDs) and organic solar cells (OSC) depends on efficient coupling between optical far field modes and the emitting/absorbing region of the device. Current approaches towards OLEDs with efficient light-extraction often are limited to single-color emission or require expensive, non-standard substrates or top-down structuring, which reduces compatibility with large-area light sources. Here, we report on integrating solution-processed nano-particle based light-scattering films close to the active region of organic semiconductor devices. In OLEDs, these films efficiently extract light that would otherwise remain trapped in the device. Without additional external outcoupling structures, translucent white OLEDs containing these scattering films achieve luminous efficacies of 46 lm W^{-1} and external quantum efficiencies of 33% (both at 1000 cd m^{-2}). These are by far the highest numbers ever reported for translucent white OLEDs and the best values in the open literature for any white device on a conventional substrate. By applying additional light-extraction structures, 62 lm W^{-1} and 46% EQE are reached. Besides universally enhancing light-extraction in various OLED configurations, including flexible, translucent, single-color, and white OLEDs, the nano-particle scattering film boosts the short-circuit current density in translucent organic solar cells by up to 70%. © *2013 AIP Publishing LLC*.
[http://dx.doi.org/10.1063/1.4807000]

I. INTRODUCTION

White-emitting OLEDs (WOLEDs) are promising candidates for the next generation of general illumination light sources.[1,2] Besides generating white light at competitive efficiency, they offer a range of features and opportunities, including the potential for low-cost manufacturing, e.g., by roll-to-roll processing,[3,4] or the possibility to fabricate large-area, intrinsically glare-free light sources that can be translucent and thus function as windows when switched off.[5–7] However, like any solid-state light source, OLEDs suffer from incomplete extraction of the light generated within the device, the fundamental reason being the higher than unity refractive index of the active, electroluminescent medium. Simulations indicate that in typical OLEDs 70%–80% of the generated photons remain confined within the device—either trapped in the substrate, guided in the organic layers and the transparent electrode (dielectric modes), or bound as surface plasmon polaritons (SPPs) at the metallic contact.[8–12] Thus, despite the high internal charge-to-photon conversion efficiencies of the latest fully-phosphorescent or triplet-harvesting OLEDs,[13–15] optimization of light extraction provides ample room for performance improvements. Furthermore, due to the presence of cavity effects, light-extraction usually depends on viewing angle. In particular for WOLEDs, this gives rise to undesired hues when looking at the device under shallow angles which poses a critical issue for the application of OLEDs in general illumination.[16] For the reverse device type, the organic solar cell (OSC), efficient absorption of incident light is critical. In principle, this can be achieved by increasing the thickness of the absorbing layers of OSCs. However, due to the limited exciton diffusion length and charge mobility within these layers, there is a trade-off between light absorption and efficient conversion of absorbed photons.[17]

Different strategies have been suggested to address the issue of inefficient light extraction and absorption. These can be broadly classified into, first, approaches involving modifications of the substrate and of external structures and, second, internal coupling schemes, where the light-managing structure is in close contact with the active region of the device. For OLEDs, the former include the application of micro-lens-arrays[18–20] or corrugated structures[2,21–23] to the backside of the substrate. The substrate-corrugation causes scattering of substrate-bound light into air and mixes up the angular components of the generated light, thus somewhat reducing undesired angle-dependent color-changes. However, the possible out-coupling enhancement is limited as such structures cannot access light trapped in dielectric and SPP modes. A way to overcome this limitation is the use of high refractive-index substrates,[1,24,25] but these are expensive and raise concerns about environmental impact and toxicity. Alternatively, a light scattering structure can be

a)Electronic mail: chungwu@cc.ee.ntu.edu.tw.
b)Electronic mail: karl.leo@iapp.de.
c)Electronic mail: malte.gather@iapp.de.

integrated in close proximity to the active layers of the device so that the dielectric and SPP modes substantially penetrate into the scattering structure.[21,26–28] However, as this potentially introduces electrical defects at rough internal interfaces, most reports on internal out-coupling structures rely on very robust, yet relatively inefficient OLED stacks. Consequently, absolute efficiencies of such structures have remained below the current state-of-the-art for devices without internal outcoupling enhancement.[29–31] Furthermore, only few reports properly acknowledge that for an internal out-coupling structure to effectively extract light from dielectric and SPP modes, the scattering length has to be significantly shorter than the decay length of these modes; otherwise no appreciable extraction is achieved before the light is largely absorbed.[32] For a typical OLED structure, the modal absorption loss $\mu_{a,\mathrm{mod}}$ of the dielectric and the plasmonic modes is estimated to be on the order of 50 and 500 mm^{-1}, respectively (see Sec. II).

Among other strategies, thin-film solar cells have used nano-particle[33] or nano-wire structures[34] as means to facilitate improved absorption or confinement of incident light. However, in the past, these techniques have not been readily applicable to OSC as the resulting surface roughness tends to cause electrical shorts in the thin active layers of OSC.

Here, we report on a facile, robust and scalable bottom-up route to integrate nano-particle based scattering layers (NPSLs) between the substrate and the anode layer of an OLED or OSC (Fig. 1(a)). We demonstrate that the solution-processable films are universally applicable to various state-of-the-art OLED structures, including single-color and white-emitting devices, devices on flexible and rigid substrates, and bottom-emitting and bi-directional translucent OLEDs. We introduce NPSLs into highly efficient OLED stacks that were optimized electrically and optically and show that the NPSL further enhances the efficiency of these stacks by more than 50% relative to reference devices without the NPSL. For WOLEDs we also find a dramatic improvement of the color-stability with respect to viewing angle and obtain nearly perfect Lambertian emission characteristics. Moreover, we show that the NPSL concept enables translucent OSC with superior short-circuit current density and efficiency.

II. EXPERIMENTAL

To fabricate the NPSLs, 0.6 g of TiO_2 nanoparticles (mean diameter 240 nm, Centron Biochemistry Technology Co., Ltd) were dispersed in 4 ml of a propylene glycol-monomethyl-ether acetate (PGMEA) solution of an optical polymer host matrix (EOC130, Everlight Chemical). (Dispersions with 0.3 g and 0.1 g of TiO_2 nanoparticles were also prepared.) 12 g of ZrO_2 particles (mean diameter 100 μm) were added to the mixture as milling objects. A homogenous dispersion was achieved by physical vibration, stirring and milling of the mixture for 24 h. Subsequently, the dispersion was filtered (pore size, 5 μm) to remove the milling particles. NPSLs were fabricated by spin-coating (1000 rpm, 40 s) onto 2 in. × 2 in. substrates. NPSLs were subsequently heat-cured (130 °C, 10 min) to remove residual solvent and

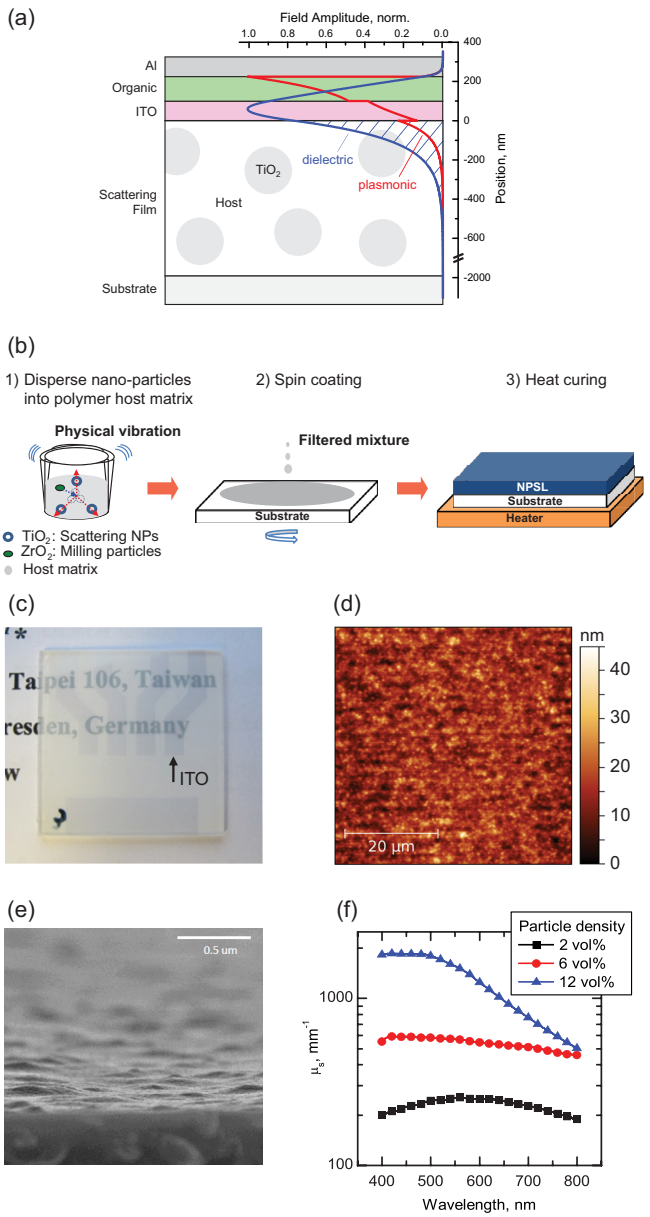

FIG. 1. Enhanced light extraction in OLEDs by nano-particle based scattering layers. (a) Schematic illustration of the operation principle: A scattering film is inserted between the substrate and the OLED stack, formed by an ITO bottom electrode, multiple organic layers and an aluminum top contact. The blue and the red line represent the field distribution of the lowest order s-polarized dielectric mode and the plasmonic mode supported by the structure (for $\lambda_0 = 520$ nm). The overlap of the evanescent tail of these bound modes with the scattering layer facilitates extraction of otherwise trapped light. Overlap of dielectric mode with scattering layer is marked by shading (diagonal blue lines). (b) Schematic illustration of the solution-based fabrication of the scattering films. After dispersing TiO_2 nanoparticles in a polymer host (1), the mixture is deposited on the substrate by spin-coating (2). A final heat-curing step removes residual solvent and planarizes the film (3). (c) Picture of the scattering film deposited on a glass substrate (electrode marked by "ITO"). (d) Atomic force microscopy image showing the surface topography of the scattering film. (e) Scanning electron microscopy image of the film under an oblique angle. (f) Effective scattering coefficient, μ_s, for scattering films with different volume fractions of TiO_2 nanoparticles.

aid the formation of a smooth film. The solid content of the original PGMEA polymer solution was 30%, yielding a concentration of TiO_2 particles (density, ~4.24 g/ml) in the final film of approximately 12 vol. % corresponding to a particle density of 20 μm^{-3}.

NPSLs were optically characterized by measuring specular transmission, i.e., the direct transmission of light incident normal to the sample surface, with a conventional UV/VIS spectrophotometer (JASCO-V570). Total transmission and total reflectance measurements were performed by attaching the coated substrates to one port of an integrating sphere and collecting either the total transmitted or the total reflected light. The integrating sphere is connected to the same UV/VIS spectrophotometer used for specular transmission measurements. The scattering coefficient is estimated from $T_{specular,NPSL}/T_{total,reference} = \exp(-\mu_s d)$, where $d = 2\,\mu$m is the thickness of the NPSL.

The scattering coefficient, μ_s, of the NPSL was simulated using an open source software implementation of Mie theory (http://omlc.ogi.edu/software/mie/) assuming spherical non-absorbing and perfectly mono-disperse particles with refractive index of 2.2 (at 520 nm vacuum wavelength) embedded in a non-absorbing, optically isotropic matrix with refractive index of 1.5 (again at 520 nm). Nominal concentration and particle diameter as described below were used without any correction factor. Effective refractive indices and electric field amplitude profiles of the dielectric and SPP modes supported by typical OLED structures were determined with a numerical one dimensional mode-solver software. The modal absorption loss is extracted from the complex effective refractive index of the mode ($\mu_{a,mod} = 4\pi\, \mathcal{I}m(n_{eff})/\lambda_0$; where $\mu_{\alpha,mod}$ is defined such that the intensity I of the mode decays over distance x as $I(x)/I_0 = \exp(-\mu_{\alpha,mod}\, x)$). The analyzed stack consisted of a glass substrate (n = 1.5), a 2 μm thick matrix polymer layer (n = 1.55), a 100 nm ITO layer (n = 1.95 + 0.0035i), 125 nm of organic (n = 1.75) and a 150 nm aluminum top-contact (n = 0.68 + 5.32i). Assuming structures with several organic layers with different refractive indices introduces only minor changes to the computed field profiles and absorption losses.

For OLED and OSC fabrication, ITO electrodes with a sheet resistance of ~50 Ω/sq were deposited on NPSLs by RF magnetron sputtering. ITO contacts were structured by a contact metal mask applied during sputtering and used without annealing. Flexible green OLEDs were fabricated on PET substrates coated with an NPSL and an ITO anode. Reference devices were fabricated on ITO coated glass substrates. The OLED stack consisted of ITO (100 nm)/TAPC (50 nm)/mCP:$Ir(ppy)_3$ (8 wt. %, 15 nm)/TPBi:$Ir(ppy)_3$ (8 wt. %, 10 nm)/TPBi (50 nm)/LiF (0.5 nm)/Al (100 nm). Bi-directional WOLEDs were fabricated on glass substrates coated with an NPSL and an ITO anode or just with an ITO contact (reference). Devices consisted of a tandem stack comprising of ITO (100 nm)/MeO-TPD: F6-TCNNQ (2 wt. %, 35 nm)/Spiro-TAD (10 nm)/4 P-NPD: $Ir(MDQ)_2$(acac) (5 wt. %, 5 nm)/4 P-NPD (5 nm)/BPhen (10 nm)/BPhen: Cs (90 nm)/Ag (0.5 nm)/MeO-TPD: F6-TCNNQ (2 wt. %, 75 nm)/Spiro-TAD (10 nm)/TCTA: $Ir(ppy)_3$: $Ir(dhfpy)_2$(acac) (91 wt. %: 8 wt. %: 1 wt. %, 5 nm)/TPBi: $Ir(ppy)_3$:$Ir(dhfpy)_2$(acac) (91 wt. %: 8 wt. %: 1 wt. %, 5 nm, Sensient/Lumtec)/TPBi (10 nm)/BPhen: Cs (60 nm)/Ag (20 nm)/Spiro-TAD (50 nm). Translucent OSCs contained a PEDOT:PSS electrode (Clevios PH1000 from Heraeus, Germany) mixed with 6 vol. % of ethylene glycol deposited directly on the NPSL. Reference devices were fabricated on ITO coated glass substrates. Both devices consisted of BF-DPB:NDP-9 (10 wt. %, 80 nm)/F4-ZnPc (5 nm)/F4-ZnPc:C60 (1:1, 65 nm, bulk hetero-junction, annealed at 100 °C)/C60 (30 nm)/BPhen (6 nm)/Al (1 nm)/Ag (15 nm)/Alq3 (50 nm). The active area of all devices was defined by the overlap between the anode and the top electrode. The organic and metal layers were deposited by thermal evaporation in a vacuum chamber with a base pressure of $<10^{-6}$ Torr. For organic materials, typical deposition rates were <1 Å s^{-1}. Doping was achieved by co-evaporation of host and dopant at independently controlled evaporation rates. The abbreviations for the chemicals used in this work have the following meaning: TAPC is di-[4-(N,N-ditolyl-amino)-phenyl]cyclohexane (Sensient); mCP is *N,N′*-dicarbazolyl-1,3-benzene (Lumtec); TPBi is 2,2′2″-1,3,5-(benzenetriyl)-tris[1-phenyl-1 H-benzimidazole] (Sensient); $Ir(ppy)_3$ is fac-tris(2-phenylpyridine) iridium (III) (Lumtec); MeO-TPD is N,N,N′,N′-tetrakis(4-methoxyphenyl)-benzidine (Sensient); F6-TCNNQ is 2,2′-(perfluoronaphthalene-2,6-diylidene)dimalononitrile (Novaled); Spiro-TAD is 2,2′,7,7′-tetrakis(N,N-diphenylamino)-9,9′-spirobifluorene (Lumtec); 4 P-NPD is N,N′-di-1-naphthalenyl-N,N′-diphenyl-[1,1′:4′,1″:4″,1‴-quaterphenyl]-4,4‴-diamine (Lumtec); $Ir(MDQ)_2$(acac) is bis(2-methyldibenzo-[f,h] quinoxaline) (acetylacetonate) iridium(III) (Lumtec); BPhen is 4,7-diphenyl-1,10-phenanthroline (ABCR); TCTA is 4,4′,4″ tris(N-carbazolyl)-triphenylamine (Sensient); $Ir(dhfpy)_2$(acac) is bis(2 -(9,9-dihexylfluorenyl)-1-pyridine) (acetylacetonate) iridium(III) (Lumtec); PEDOT:PSS is poly(3,4-ethylenedioxythiophene):poly(styrenesurfonate), BF-DPB is N,N′-((diphenyl-N,N′-bis)9,9,-dimethyl-fluoren-2-yl)-benzidine (synthesized in-house); NDP-9 is a proprietary p-dopant (Novaled), F4-ZnPc is fluorinated zinc phthalocyanine (BASF).

To record current/voltage/forward-luminescence characteristics of OLEDs, a source-measurement unit, a calibrated Si photodiode, and a fiber spectrometer calibrated for absolute intensity were used. Luminous efficacy and external quantum efficiency were determined with an integrating sphere setup (ø = 500 mm). Where noted, a glass half-sphere was mounted to the substrate and the cover glass using an index-matching gel. The angle dependence of the emission characteristics was recorded with a custom-built goniometer setup equipped with a calibrated fiber spectrometer.

The current–voltage characteristics of OSCs were measured with a source measurement unit under an AM 1.5 G sun simulator (16 S-003-300-AM1.5 from Solar Light Co., USA). The values of short circuit current are normalized to 100 mW cm^{-2}.

III. RESULTS AND DISCUSSION

The NPSLs are based on titanium dioxide nano-particles (TiO_2-NPs, mean diameter 240 nm, refractive index, ≈ 2.2) embedded in a transparent optical polymer matrix (refractive index, 1.53) at a concentration of 12 vol. %. Due to the large refractive index contrast between matrix and TiO_2-NPs, strong scattering is expected. Both matrix and TiO_2-NPs

TABLE I. Thickness, surface roughness and optical characteristics of a nano-particle based scattering layer on glass. Layers comprise of 12 vol. % of TiO_2 nanoparticles dispersed in an optical polymer matrix. Corresponding values for a reference layer of matrix polymer alone, without scattering particles. Optical characteristics measured at $\lambda_0 = 520\,\text{nm}$.

	Thickness, μm	Roughness rms, nm	T_{total}, %[a]	T_{diffuse}, %[b]	T_{specular}, %[c]	R_{total}, %[d]	$\mu_s\,\text{mm}^{-1}$ [e]
Nano-particle scattering layer	2	4.5	50.6	47.6	3.0	42.2	1709
Matrix polymer film	1.4	0.6	91.6	0.2	91.4	8.4	1.5

[a]Total transmission.
[b]Diffuse transmission ($T_{diffuse} = T_{total} - T_{specular}$).
[c]Specular transmission.
[d]Total reflectance.
[e]Scattering coefficient.

show low absorption and excellent optical and thermal stability. Figure 1(b) schematically illustrates the solution-based fabrication of NPSLs. The resulting 2 μm thick films have a hazy, highly scattering, and uncolored appearance (Fig. 1(c)). They show good adhesion and mechanical stability, thus readily facilitating the deposition of electrodes and organic layers on top. Atomic force microscopy measurements (Fig. 1(d)) and scanning electron microscopy data (Fig. 1(e)) show no indication of TiO_2-NP agglomeration. The films feature low surface roughness (4.5 nm, root-mean-square, across a $50 \times 50\ \mu\text{m}^2$ area) and are free of spike-type inhomogeneities, suggesting that the polymer matrix completely encloses the TiO_2-NPs.

The NPSLs were optically characterized by measurements of specular, diffuse, and total transmittance (T_{specular}, T_{diffuse}, T_{total}) as well as total reflectance (R_{total}) (Table I). With respect to films of the pure matrix polymer without TiO_2-NPs, specular transmission is dramatically reduced, while diffuse transmission increases from <1% to >40%. Notably, very little light is absorbed in the structure ($T_{\text{total}} + R_{\text{total}} > 90\%$), indicating excellent optical quality. Based on the specular and diffuse transmission data, we estimate the effective scattering coefficient, μ_s, for light propagating within the NPSL to $1700\,\text{mm}^{-1}$ (see Sec. II). This value is in excellent agreement (deviation, <10%) with the result of Mie-theory,[35] assuming homogenously distributed spherical TiO_2-NPs at the nominal concentration and size. We found that the effective scattering coefficient tends to increase with increasing concentrations of TiO_2-NPs in the film (Fig. 1(f)). The films with 12 vol. % of TiO_2-NPs represent the highest particle concentration that can presently be produced without compromising film roughness and homogeneity.

The evanescent tail of the guided modes supported by typical OLED structures extends substantially into the region beneath the bottom electrode, i.e., into the region where the NPSL is located in our devices. Figure 1(a) shows the calculated field distribution of the lowest order s-polarized dielectric mode in a typical OLED stack (at $\lambda_0 = 520\,\text{nm}$, see Sec. II). The effective refractive index of this mode is computed to $n_{\text{eff,diel}} = 1.71$, the modal absorption is $\mu_{\alpha,\text{diel}} = 80\,\text{mm}^{-1}$ and the spatial mode overlap of the mode with the NPSL is $\Gamma_{\text{diel}} > 30\%$. (Here, spatial mode overlap refers to the fraction of the mode volume that resides within the NPSL, see area shaded with diagonal lines in Fig. 1(a).) Interestingly, even modes of plasmonic nature show sizeable overlap with the NPSL; in the case illustrated in Fig. 1(a), $\Gamma_{\text{SPP}} > 10\%$ ($n_{\text{eff,SPP}} = 1.87$, $\mu_{\alpha,\text{SPP}} = 630\,\text{mm}^{-1}$). For the dielectric mode, the modal scattering coefficient, $\mu_{\text{s,diel}} = \Gamma_{\text{diel}}\,\mu_s$, clearly exceeds the modal absorption $\mu_{\alpha,\text{diel}}$, indicating that light confined in this mode is completely

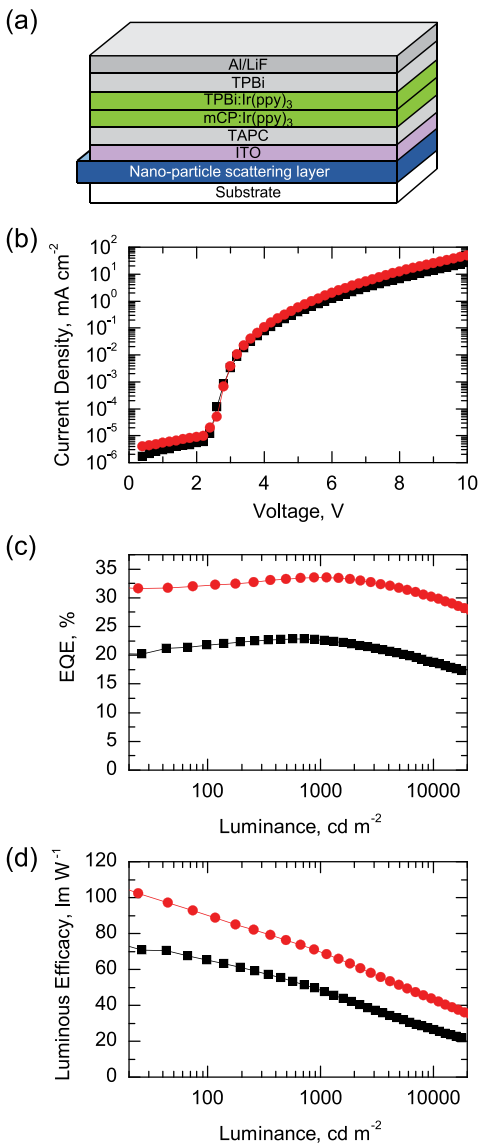

FIG. 2. Flexible phosphorescent green OLED with embedded scattering film. (a) Device structure, (b) current density-voltage (IV) characteristics, (c) external quantum efficiency, and (d) luminous efficacy versus luminance for an OLED containing a scattering film (●) and for a reference device (■) without the light extraction structure.

scattered. For the plasmonic mode, the modal scattering coefficient, $\mu_{s,SPP}$, and the absorption coefficient, $\mu_{\alpha,SPP}$, are comparable; for these modes scattering competes with absorption.

In the following, we discuss examples of OLED and OSC structures comprising NPSLs that promote increased out-coupling and light absorption, respectively. First, we illustrate the applicability of the NPSL concept to rollable mobile displays by studying single-color, green-emitting phosphorescent OLEDs deposited on flexible PET foil substrates. PET foils were coated with an NPSL and an indium tin oxide (ITO) thin film electrode. Reference devices without the NPSL were also prepared. A highly efficient OLED stack based on the green phosphorescent emitter $Ir(ppy)_3$ embedded in layers of TPBi and mCP was deposited on top of these substrates. Figure 2(a) shows a schematic illustration of the device stack.

A major concern with many internal out-coupling structures is that local thickness variations introduced by these structures negatively affect the electrical device properties,

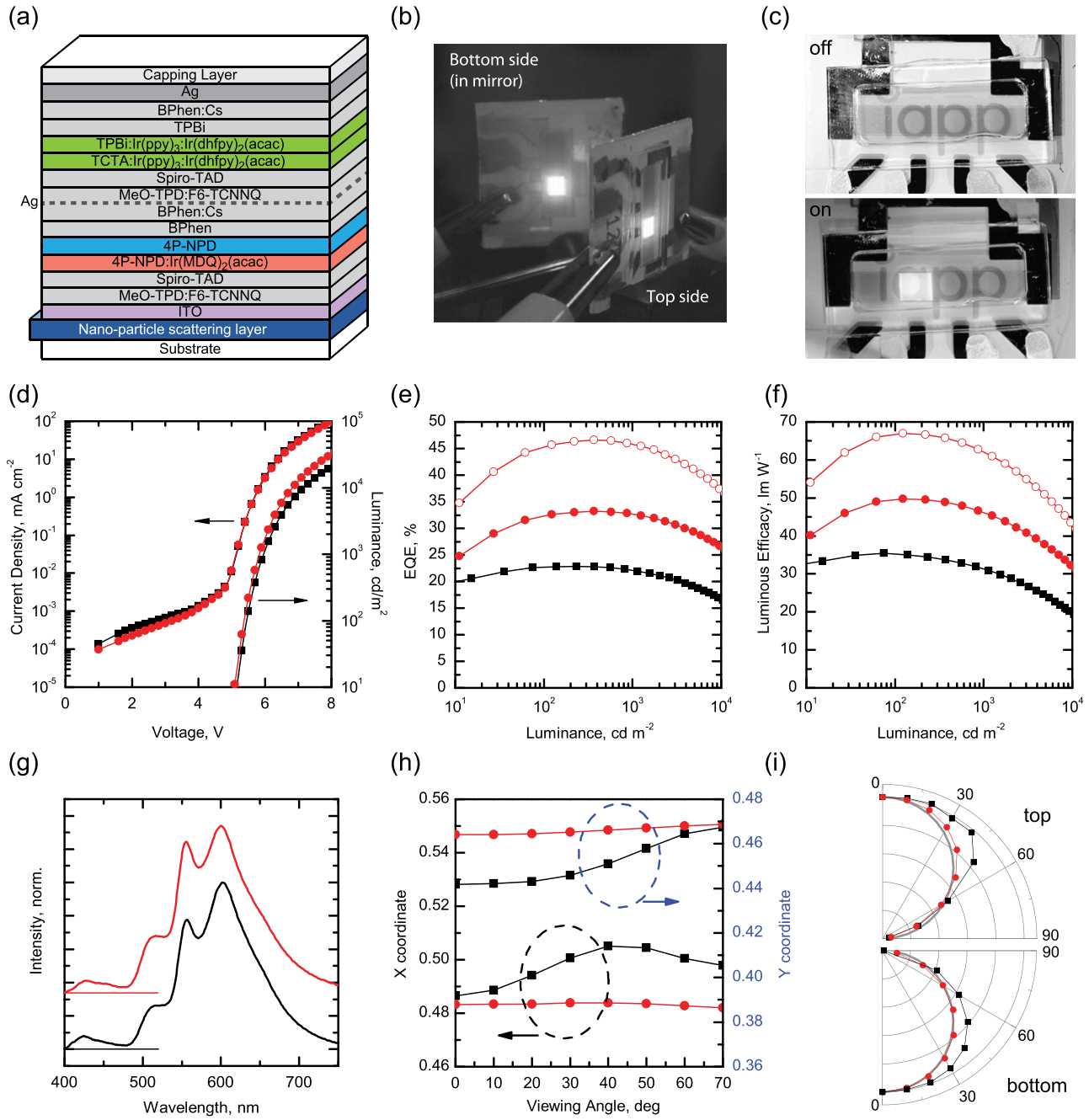

FIG. 3. Scattering layers improve efficiency and color stability of translucent white OLED. (a) Structure of the triplet harvesting tandem OLED stack used to demonstrate the effect of the scattering layer. Images of operating devices, illustrating (b) bi-directional emission and (c) translucence. (d) Luminance- current density-voltage (LIV) characteristics, (e) external quantum efficiency, and, (f) luminous efficacy versus luminance for an OLED containing internal scattering layer (●), for a device with scattering layer and external index-matched half-spheres (○) and for a reference device without light extraction structures (■). (g) Angle-integrated electroluminescence spectrum of device with (—) and without (—) scattering layer and (h) change of CIE coordinates with viewing angle for the device with (●) and without (■) scattering layer. (i) Angular dependence of normalized luminance for device with (●) and without (■) scattering layer. Grey line represents an ideal Lambertian emitter.

resulting in parasitic leakage current and high local electrical stress. For the NPSLs, this issue is mitigated by thoroughly dispersing the TiO_2-NPs in the polymer matrix and heat-curing of the final film. As a result, the leakage current in these devices is nearly equal to that in NPSL-free reference devices (Fig. 2(b)). At the same time, the external quantum efficiency (EQE) and the luminous efficacy of the devices are increased by ~50% relative to the reference device (Figs. 2(c) and 2(d)). Notably, the reference OLED without NPSL already reached 22.5% EQE; this is close to the theoretical maximum achievable in conventional bottom-emitting devices.[11] The NPSL device achieves 34% EQE and a luminous efficacy of 69 lm W^{-1} (at 1000 cd m^{-2}; without application of additional external out-coupling schemes). Due to the slow efficiency roll-off, the EQE remains at 30%, even at high luminance of 10 000 cd m^{-2}.

The effectiveness of many light-extraction schemes, including those based on micro-cavities, thin film capping layers, or Bragg-gratings, is highly wavelength dependent. As a result, such approaches are not readily compatible with white-emitting devices. By comparison, the scattering of nanoparticles in principle shows weak wavelength dependence over visible wavelengths, thus promising homogenous improvement of light-extraction across the emission range of WOLEDs. To test this, we combine the NPSL with a highly efficient tandem WOLED stack that makes use of the triplet harvesting concept and uses doped charge transport and charge generation layers. The used structure is derived from the stack reported in Ref. 36 but comprises a semi-transparent top-electrode with a dielectric capping layer (Fig. 3(a)). The obtained devices emit through both the bottom and the top electrode (Fig. 3(b)) and are translucent when turned off (Fig. 3(c)), which opens up possibilities for new applications in lighting. Again an optimized stack architecture was selected to ensure that performance enhancements are true scattering effects and not artifacts of electrical or optical cavity tuning. At a luminance of 1000 cd m^{-2}, the EQE and luminous efficacy of reference devices without NPSL reach 22% and 32 lm W^{-1}, respectively, which is very similar to the numbers previously reported for conventional bottom emitting WOLEDs based on the same stack. Like in the monochromatic devices discussed above, the presence of the NPSLs had no significant impact on the electrical device properties. The semi-log plot of the current-voltage characteristics shows that the leakage current remains unaffected by the introduction of the scattering film (Fig. 3(d)). However, compared to a reference without NPSL, the EQE and luminous efficacy are markedly increased. Figures 3(e) and 3(f) show the performance for the combined emission from the top and the bottom side of the devices. (The luminance ratio, L_{bottom}/L_{top}, balances from 1.9: 1 for the reference to 1.5: 1 for the NPSL device.) At a luminance of 1000 cd m^{-2}, EQE and luminous efficacy reach values of 33% and 46 lm W^{-1}, respectively. These values are the best reported for translucent white OLEDs until now and furthermore represent the highest numbers for any white OLED structure deposited on a conventional substrate (i.e., with a refractive index around 1.5) that is described in the open literature. By attaching glass half spheres, EQE and luminous efficacy can be enhanced further to 46% and 62 lm W^{-1}, respectively.

The electroluminescence spectrum is only marginally affected by the introduction of the NPSL (Fig. 3(g)) illustrating the weak wavelength dependence of the outcoupling enhancement provided by the NPSL. However, while the spectrum and color of the light emitted by the reference device change strongly with the viewing angle, the emission from the NPSL device is extremely stable over all angles (Fig. 3(h)). Strong changes in spectrum and perceived color with viewing angle are common for many WOLED structures. In particular, efficient tandem WOLED stacks are usually characterized by a relatively thick cavity that gives rise to strong shifts of the cavity resonance with angle. In the present case, the maximum change in the Commission Internationale de l'Éclairage (CIE) coordinates over the 70° forward viewing cone is $\Delta(x, y) \approx (0.019, 0.026)$ in the reference device and $<(0.001,0.005)$ in the NPSL-OLED. The latter is considerably smaller than one MacAdam ellipse,[37] i.e., the human eye does not notice any change in hue when the OLED is tilted. The NPSL approach thus solves the long-standing color stability issue in WOLEDs. Additionally, adding the NPSL to the OLED stack results in a nearly perfect Lambertian angle-dependence of the device luminance (Fig. 3(i)).

Finally, we demonstrate the application of the NPSL concept to translucent OSCs adapting an opaque small-molecule

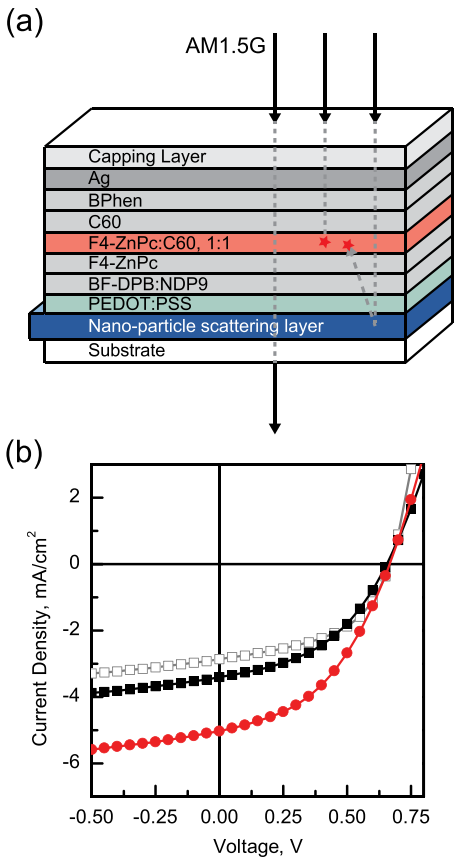

FIG. 4. Translucent organic solar cells with improved short circuit current. (a) Device structure of translucent small molecule organic solar cells with F4-ZnPc:C60 bulk hetero-junction. Arrows illustrate the possible light paths, i.e., direct transmission, direct absorption, and absorption after scattering. (b) Current density versus voltage characteristics of organic solar cell with (●) and without (■) the scattering layer under AM 1.5 G irradiation with an intensity of 100 mW cm^{-2}. Data for a reference device with ITO electrode instead of PEDOT:PSS electrode are also shown (□).

TABLE II. Figures of merit for translucent organic solar cells with and without scattering layer. Data listed are upon top illumination for cells with and without the scattering layer and for a reference cell with an ITO electrode.

	V_{OC}, V[a]	J_{SC}, mA/cm^2[b]	*FF* %[c]	*Eff.* %[d]
w/o scattering, PEDOT	0.66	3.4	43.8	0.98
with scattering, PEDOT	0.67	5.0	43.6	1.46
w/o scattering, ITO	0.67	2.9	49.3	0.94

[a]Open-circuit voltage.
[b]Short circuit current.
[c]Fill factor.
[d]Power conversion efficiency.

based OSC stack.[38] Achieving efficient absorption of the incident light is particularly challenging in translucent OSCs as the absence of a rear reflector limits the interaction of incident light with the OSC to a single pass through the absorbing layer of the device. Figure 4(a) shows a schematic of the translucent NPSL-OSC investigated here. Here, the ITO electrode used in the OLED stacks was replaced by a highly conductive solution-processable organic PEDOT:PSS electrode.[39] The current-voltage characteristics of the NPSL-OSC under AM1.5 G illumination show a 1.7-fold higher short-circuit current density than an NPSL-free reference cell using an ITO electrode (Fig. 4(b)). As a result, the power conversion efficiency increases by 55% relative to the reference device (Table II). We attribute this increase to the fact that the highly scattering and nearly non-absorbing NPSL feeds a substantial fraction of the light that is not absorbed during the first pass through the OSC back into the device. This allows more efficient harvesting of the incident photons while still transmitting a substantial fraction of the incident light ($T_{total} \approx 30\%$).

IV. CONCLUSION

We have introduced a universal, light-scattering based platform technology to greatly enhance the out-coupling efficiency in various types of OLEDs as well as the light harvesting in OSCs. Our approach is compatible with a wide range of substrates, electrodes and stack architectures, including flexible substrates as well as bi-directionally emitting, translucent stacks. NPSLs can be fabricated in a simple, solution-based, lithography-free, bottom-up process and significantly enhance the performance of highly efficient, pre-optimized, state-of-the-art OLED stacks. Compared to other approaches, the scattering efficiency is weakly wavelength dependent. NPSLs are thus most suitable for light extraction in WOLEDs and photon redistribution in OSCs. The performance can be improved further if the NPSLs are optimized to achieve complete scattering of light bound in plasmonic modes. This can be achieved either by enhancing the scattering coefficient or by increasing the spatial overlap of the scattering structure with the plasmon modes.

ACKNOWLEDGMENTS

This work was supported by the German BMBF (13N11060, project R2FLEX) and the National Science Council and Ministry of Education of Republic of China (Taiwan) (NSC-99-2221-E-002-118-MY3 and 10R70607). H.-W.C. and J.L. gratefully acknowledge financial support as fellows of the Deutscher Akademischer Austauschdienst (DAAD) and the Alexander von Humboldt Foundation (AvH), respectively. M.C.G. acknowledges support from the Daimler and Benz Foundation. The authors are grateful to Tae Hyun Gil and Sebastian Franke (Fraunhofer COMEDD) for ITO sputtering, to Tobias Mönch for support with AFM, Nils Kronenberg for optical characterization and to Novaled AG for access to the integrating sphere setup.

[1]S. Reineke, F. Lindner, G. Schwartz, N. Seidler, K. Walzer, B. Lüssem, and K. Leo, Nature **459**, 234–242 (2009).
[2]Y. Sun and S. R. Forrest, Nature Photon. **2**, 483–970 (2008).
[3]A. Köhnen, N. Riegel, J. Kremer, H. Lademann, D. C. Müller, and K. Meerholz, Adv. Mater. **21**(8), 879–884 (2009).
[4]T.-H. Han, Y. Lee, M.-R. Choi, S.-H. Woo, S.-H. Bae, B. H. Hong, J.-H. Ahn, and T.-W. Lee, Nature Photon. **6**, 105–110 (2012).
[5]V. Bulovic, G. Gu, P. Burrows, S. Forrest, and M. Thompson, Nature **380**, 29 (1996).
[6]J. Meyer, P. Görrn, S. Hamwi, H. H. Johannes, T. Riedl, and W. Kowalsky, Appl. Phys. Lett. **93**, 73308 (2008).
[7]J. Lee, S. Hofmann, M. Furno, M. Thomschke, Y. Kim, B. Lüssem, and K. Leo, Opt. Lett. **36**(8), 1443–1448 (2011).
[8]V. Bulovic, V. Khalfin, G. Gu, P. Burrows, D. Garbuzov, and S. Forrest, Phys. Rev. B **58**(7), 3730 (1998).
[9]K. Neyts, Appl. Surf. Sci. **244**(1), 517–523 (2005).
[10]C. L. Lin, T. Y. Cho, C. H. Chang, and C. C. Wu, Appl. Phys. Lett. **88**, 81114 (2006).
[11]R. Meerheim, M. Furno, S. Hofmann, B. Lüssem, and K. Leo, Appl. Phys. Lett. **97**(25), 253305 (2010).
[12]S. Mladenovski, S. Hofmann, S. Reineke, L. Penninck, T. Verschueren, and K. Neyts, J. Appl. Phys. **109**(8), 083114 (2011).
[13]H. Sasabe, J. Takamatsu, T. Motoyama, S. Watanabe, G. Wagenblast, N. Langer, O. Molt, E. Fuchs, C. Lennartz, and J. Kido, Adv. Mater. **22**(44), 5003 (2010).
[14]E. L. Williams, K. Haavisto, J. Li, and G. E. Jabbour, Adv. Mater. **19**, 197–202 (2007).
[15]Y. Sun, N. Giebink, H. Kanno, B. Ma, M. Thompson, and S. Forrest, Nature **440**, 908–920 (2006).
[16]A. Isphording and M. Pralle, Org. Electron. **11**(12), 1916–3835 (2010).
[17]B. C. Thompson and J. M. J. Fréchet, Angew. Chem., Int. Ed. Engl. **47**(1), 58–77 (2008).
[18]S. Möller and S. Forrest, J. Appl. Phys. **91**, 3324 (2002).
[19]C. Madigan, M. H. Lu, and J. Sturm, Appl. Phys. Lett. **76**(13), 1650–3302 (2000).
[20]M. Thomschke, S. Reineke, B. Lüssem, and K. Leo, Nano Lett. **12**(1), 424–432 (2012).
[21]W. H. Koo, S. M. Jeong, F. Araoka, K. Ishikawa, S. Nishimura, T. Toyooka, and H. Takezoe, Nature Photon. **4**(4), 222–448 (2010).
[22]Y. J. Lee, S. H. Kim, J. Huh, G. H. Kim, Y. H. Lee, S. H. Cho, Y. C. Kim, and Y. R. Do, Appl. Phys. Lett. **82**, 3779 (2003).
[23]J. Feng, T. Okamoto, and S. Kawata, Opt. Lett. **30**(17), 2302–2306 (2005).
[24]S. Mladenovski, K. Neyts, D. Pavicic, A. Werner, and C. Rothe, Opt. Express **17**(9), 7562–7632 (2009).
[25]B. J. Scholz, J. Frischeisen, A. Jaeger, D. S. Setz, and W. Brütting, Opt. Express **20**(102), A205 (2012).
[26]H. Peng, Y. Ho, X. Yu, and H. Kwok, J. Appl. Phys. **96**, 1649 (2004).
[27]M. Fujita, K. Ishihara, T. Ueno, T. Asano, S. Noda, H. Ohata, T. Tsuji, H. Nakada, and N. Shimoji, Jpn. J. Appl. Phys. **44**, 3669 (2005).
[28]Y.-C. Kim and Y. Do, Opt. Express **13**(5), 1598–2201 (2005).
[29]Z. Wang, Z. Chen, L. Xiao, and Q. Gong, Org. Electron. **10**(2), 341–686 (2009).
[30]B. Riedel, Y. Shen, J. Hauss, M. Aichholz, X. Tang, U. Lemmer, and M. Gerken, Adv. Mater. **23**(6), 740–745 (2011).
[31]C. S. Choi, S. M. Lee, M. S. Lim, K. C. Choi, D. Kim, D. Y. Jeon, Y. Yang, and O. O. Park, Opt. Express **20**(6), A309–A318 (2012).
[32]J. Choi, T.-W. Koh, S. Lee, and S. Yoo, Appl. Phys. Lett. **100**, 233303 (2012).

[33]S. Ito, T. N. Murakami, P. Comte, P. Liska, C. Grätzel, M. K. Nazeeruddin, and M. Grätzel, Thin Solid Films **516**(14), 4613–4619 (2008).
[34]E. Garnett and P. D. Yang, Nano Lett. **10**(3), 1082–1087 (2010).
[35]W. Wiscombe, Appl. Opt. **19**(9), 1505–1514 (1980).
[36]T. C. Rosenow, M. Furno, S. Reineke, S. Olthof, B. Lussem, and K. Leo, J. Appl. Phys. **108**(11), 113113 (2010).
[37]D. L. MacAdam, J. Opt. Soc. Am. **33**(1), 18–44 (1943).
[38]J. Meiss, A. Merten, M. Hein, C. Schuenemann, S. Schäfer, M. Tietze, C. Uhrich, M. Pfeiffer, K. Leo, and M. Riede, Adv. Funct. Mater. **22**, 405–414 (2012).
[39]Y. H. Kim, C. Sachse, M. L. Machala, C. May, L. Müller-Meskamp, and K. Leo, Adv. Funct. Mater. **21**, 1076 (2011).